Biotic and abiotic retention, recycling, and remineralisation of metals in the ocean

Revised Progress Article for Nature Geoscience

2 December 2016

Philip W. Boyd[1,2], Michael J. Ellwood[3], Alessandro Tagliabue[4] and Benjamin S. Twining[5]

Affiliations

[1]Institute for Marine and Antarctic Studies, University of Tasmania, Hobart, Tasmania, Australia

[2]Antarctic Climate and Ecosystems CRC, University of Tasmania, Australia

[3]Research School of Earth Sciences, The Australian National University, Canberra, ACT 0200 Australia

[4]School of Environmental Sciences, University of Liverpool, Liverpool, UK

[5]Bigelow Laboratory for Ocean Sciences, East Boothbay, Maine, USA

Abstract

Trace metals shape both the biogeochemical functioning and the biological structure of oceanic provinces. Trace metal biogeochemistry has primarily focused on modes of external supply of metals from aeolian, hydrothermal, sedimentary and other sources. However, metals also undergo internal transformations such as abiotic and biotic retention, recycling, and remineralization. The role of these internal transformations in metal biogeochemical cycling is now coming into focus. First, the retention of metals by biota in the surface ocean for days, weeks, or months depends on taxon-specific metal requirements of phytoplankton, and on the ultimate fate of phytoplankton, that is viral lysis, senescence, grazing, and/or export to depth. Rapid recycling of metals in the surface ocean can extend seasonal productivity by maintaining higher levels of metal bioavailability, compared to the influence of external metal input alone. As metal-containing organic particles are exported from the surface ocean, different metals exhibit distinct patterns of remineralization with depth. These patterns are mediated by a wide range of physico-chemical and microbial processes such as the ability of particles to sorb metals, and are influenced by the mineral and organic characteristics of sinking particles. We conclude that internal metal transformations play an essential role in controlling metal bioavailability, phytoplankton distributions, and the subsurface resupply of metals.

Trace metals such as iron set primary productivity across much of the ocean[1,2]. Other metals, including zinc and cobalt, play more targeted physiological roles linked to specific biogeochemical cycles[3,4]. Much emphasis in metal biogeochemistry has been placed on the identification of external supply mechanisms[5,6]. However, in the case of iron much of this supply, such as episodic dust plumes, may be chemically inaccessible[7] and/or biologically unavailable[8]. Long-standing investigations of nitrogen and phosphorus biogeochemistry[9] established that internal recycling through efficient biological retention sustains productivity. Likewise, solubilisation of elements from sinking particles, termed remineralisation, replenishes nutrient inventories at depth[10], which are seasonally re-supplied to surface waters by mixing. Here, we exploit newly available insights to explore the abiotic and biotic mechanisms that underpin internal metal cycling, focussing on iron as the best-characterised metal[11], but drawing on illustrative examples for other metals. We contrast recycling patterns between trace- and macro-nutrients, and link the former to external supply mechanisms of metals to complete their biogeochemical cycles.

Trace metals have fundamentally different chemistry (speciation, reactivity, complexation[11]) than macro-nutrients[12], and thus have distinctive modes of external supply and internal recycling, with implications for the contribution of recycling versus external supply in supporting productivity (i.e., the *f* ratio[12], see later). Additionally, macro-nutrients support macromolecular synthesis[12] whereas metals drive enzymatic catalysis[13]. These distinct metabolic roles probably account for different taxon-specific requirements for metals[14], a trend not evident for macro-nutrients[15]. While some taxa target particular forms of macronutrients (e.g., *Prochlorococcus/*ammonium; *Synechococcus/*nitrate[16]), such

preferences are poorly-defined for metals, due to uncertainties such as how metal-binding ligands influence bioavailability[11].

We detail important advances across four specific themes: (i) pelagic iron retention/recycling; (ii) ratio of new/recycled iron and modes of supply; (iii) observed versus modelled mesopelagic metal remineralisation; and (iv) controls on subsurface metal remineralisation. Our understanding has advanced substantially from prior reviews[17] (S-Figure 1), catalysed by GEOTRACES[18], and we highlight insights from GEOTRACES process studies[19,20], surveys[8,21,22], GEOTRACES-inspired modelling[23,24], along with other recent[7,25,26], and prior (corroborative) research[27,28]. FeCycle II, a 12-day quasi-Lagrangian GEOTRACES process-study[19] characterised by an unprecedented combination of direct measurements of pelagic recycling[19,29] and subsurface metal remineralisation[29,30], serves to link our specific themes.

Drivers of pelagic metal retention and recycling

Retention of externally-supplied metals, by abiotic and biotic mechanisms, within surface waters is a prerequisite for internal cycling (for iron see Figure 1). External supply largely occurs over winter[31], with subsequent episodic supply[5,7]. For example, iron is initially retained in surface waters by excess ligands, a trend evident across GEOTRACES sections[22,32], regardless of the mode of external supply. Spring-time biological acquisition of iron[19,20] results in both the retention[29], and loss to depth[29,30] of this 'winter reserve' stock. Mechanisms including viral activity (lysis[19], ligands[33]) and grazing[19] internally mobilise this biologically-retained iron. Abiotic mechanisms play a key role in retaining episodically-supplied iron, from dust deposition[5] (or passing eddies[7]), through rapid 'cascades' between particulate and soluble forms[7], photochemically-mediated dissolution of colloids[34] and the

putative mechanism of transformation to inorganic iron colloids[21] (Figure 1). Different supply modes influence taxon-specific biological acquisition strategies: episodic supply can stimulate microbial siderophore production[25,26], whereas aerosols are transformed by phagotrophy[35] and/or active transport (diazotrophs[36]), and vertical diffusive supply (potentially colloidal iron[7]) is targeted by phytoplankton at depth[37].

A major advance in understanding pelagic internal cycling (S-Figure 1) is determining how the biological ferrous wheel[38] is structured by the intersection of taxon-specific iron requirements[39] (i.e., quotas, total intracellular metal, mol/cell) and storage abilities[40] with distinct taxon-specific pathways and 'fates' of the biologically-retained metal (i.e. grazing/lysis/cell death/sinking)[29] (Figure 1). Hence, the wide-ranging acquisition strategies, employed by phytoplankton[41], drive differences in the retention and recycling efficiency of each element. Other metals such as nickel have differing characteristics from iron that influence distinct physiological needs and acquisition (S-Table 1). This range of acquisition mechanisms enables taxa with different metal requirements, which arise from specific metabolic needs[13,39], use efficiencies[42], and/or cell sizes/abundances[29], to co-exist. A critical unknown is how abiotic and biotic retention mechanisms interact (Figure 1). Although there have been major advances in elucidating abiotic[7,21,34] and biotic[25,26,29,33] retentive mechanisms, our understanding of the latter is more advanced. Ligands[25,26,33] may be a key linkage between mechanisms (Figure 1), however additional pathways will probably connect abiotic and biotic processes, an emerging theme across geomicrobiology[43].

What proportion of 'new' trace metal inventories can be retained by biota? During FeCycle II[19] mixed-layer dissolved iron decreased from ~0.5 to 0.1 nmol L^{-1}, but the biotic iron

inventory, based on quotas quantified with Synchrotron-X-Ray-Fluorescence (SXRF) cell-mapping[8,30], remained ~0.1 nmol L^{-1} throughout, and its rapid recycling extended seasonal productivity[19]. This study[19] suggests limits on the proportion of metal inventories biota can access and recycle, likely constrained by temperature-dependent bounds on growth/grazing rate, and/or lags in predator/prey couplings (e.g., gut passage). Moreover, not all of dissolved metal inventories may be available to all taxa[29].

New versus recycled metals and ocean productivity

The *f*e ratio describes the contribution of externally-supplied iron to biological uptake relative to that supported by both externally-supplied and internally-cycled iron[44] and hence is analogous to the *f* ratio for nitrogen[12]. Calculation of the *f*e ratio requires detailed estimates of both biological iron demand and recycling (S-Figure 1). Emerging datasets from GEOTRACES process studies[19,20] enable the relationship between the *f*e ratio and different modes of supply to be probed (Figure 2). Initial *f*e ratio estimates were from subantarctic low-iron waters where, despite invariant dissolved iron vertical profiles, ~90% of productivity was fuelled by internal cycling[44].

A major advance is the recognition that *f*e ratios change with locale, season and regional inventories (S-Figure 1). Recycled iron is less important in high-iron waters sustained by upwelling[20,45] compared with that supplied by transient 'winter-reserves' (Figure 2A,B). *f*e ratios of ~1 were evident off Kerguelen at the onset of the diatom bloom[20], and were ~0.5 after one month of bloom development[45]. In contrast, subtropical Pacific waters[29] revealed

rapid removal of externally-supplied iron (i.e., decreased *f*e ratios) during the transition to summer oligotrophy (Figure 2B).

Summer iron stocks are enhanced in subtropical Atlantic and Pacific waters via episodic dust inputs (Figure 2C). Sustained high iron[7, 28] suggests either a biological surfeit (i.e., indicative of high *f*e ratio's, no available data) or that this iron is chemically inactive[7,8] or biologically inaccessible[8] due to light and/or phosphate limitation[2]. Despite regional differences in dissolved iron stocks and *f*e ratios (Figure 2), surprising uniformity in biotic iron inventories emerges across contrasting sites[29]. This raises questions such as: can recycled iron (supplying 50-90% of demand) subsidise cells with high requirements (picoprokaryotes[39])? If some taxa target episodically-supplied iron (Figure 1), do others focus on recycled forms? If so, does iron speciation dictate such taxon specialisation?

Subsurface remineralisation length-scales

Sinking particles fuel the biological pump, and transformations attenuate particle flux with depth, replenishing dissolved nutrients[10] and setting nutricline depths[31]. Remineralisation length-scales (i.e., the attenuation (at some rate k (s^{-1})) of the downward particulate flux of an element settling gravitationally (speed ω (m s^{-1})) is defined by ω/K (m)), vary among major elements, causing vertical-decoupling at depth[10]. Length-scales also vary between metals (Table 1A). Remineralisation length-scales are generally longer for metals, relative to macro-nutrients[27], as metals comprise both lithogenic (relatively refractory) and biogenic (labile) components of sinking heterogeneous particles (Figure 3). Indeed, for copper, the sinking flux is essentially a 'lithogenic throughput' with little flux attenuation (S-Table 1). Hence, directly comparing remineralisation length-scales between elements in heterogeneous particles is problematic.

A study targeting export from a diatom-dominated bloom[30] circumvented the lithogenic influence on remineralisation by focusing analytically on diatoms. Two-dimensional elemental maps of the dominant diatom species revealed depth-dependent elemental shifts in the cellular and structural components (S-Figure 2A, Figure 3A). Significant differences between remineralisation of major elements (e.g., sulfur/silicon) and between trace elements (e.g., iron and zinc) emerged (Table 1A). Such studies[27,30] use the power of spatial associations between elements in individual particles to explore if remineralisation patterns are coupled (S-Figure 2A/B). Spatial co-location between major elements was evident in surface waters only, indicative of selective remineralisation and decoupling in the breakdown of major and trace elements with depth[30]. These advances provide the detailed mechanisms needed to better understand basin-scale cycling of major and trace elements using global ocean models (S-Figure 1).

Observed remineralisation length-scales are compared with state-of-the-art model simulations[23] in Table 1. PISCES[23] reflects observed trends in remineralisation (carbon/phosphorus length-scales <iron<silicon), but simulates a shorter length-scale globally for iron than is observed (Table 1B). As iron remineralisation in all current models[23,24] is tied to phosphorus, the ~two-fold longer remineralisation length-scale for iron versus phosphorus arises, *in silico*, from additional scavenging and colloidal pumping of remineralised iron onto particles. Observations suggest that models underestimate by four- to ten-fold iron remineralisation length-scales (Table 1A), affecting projections of nutrient resupply stoichiometry and ferricline depth[31] (S-Table 1). Future models must consider additional factors including distinct particulate pools (e.g. biogenic/lithogenic) in setting remineralisation lengthscales.

Subsurface controls on metal remineralisation

A better understanding of why element nutriclines vary[31] requires mechanisms to decouple remineralisation (S-Table 1). For macro-nutrients, mechanisms include preferential microbially-mediated nitrogen remineralisation (c.f. carbon) to meet nutritional requirements[46]. Elemental associations with different cellular components (e.g., membranes) probably influence their targeted regeneration by substrate-specific bacterial enzymes (Figure 3A). For sinking diatoms[30], more cellular P/Ni/Zn/S was remineralised compared to iron (suggesting re-adsorption due to irons' high particle reactivity[47]) and silicon (no bacterial demand means dissolution requires prior carbon solubilisation[48]) by 200 m. This study[30] provides novel linkages between elements, their biochemical role, cellular location, metal-specific microbial enzymes, and hence differential, targeted remineralisation (S-Figures 1,2).

Heterogeneous particles often dominate the sinking assemblage but are difficult to study individually (S-Figure 2B/C). Figure 3 offers a conceptual approach to jointly consider disparate biotic/abiotic mechanisms (c.f. geomicrobiology[43]) used independently to derive chemical[49] or biological[50] rate constants for particle breakdown. The fates of particulate biogenic iron, zinc and phosphorus diverge (Figure 3), because they each may encounter a range of different biological (solubilisation) and physical ((dis)aggregation) transformation mechanisms, such as for iron which likely sorbs onto (i.e., scavenged) and desorbs from particles[47,49]. Moreover, once desorbed, iron can be re-sorbed to particles[49] and/or consumed (particle-attached bacteria). It is also highly likely that abiotically-scavenged iron can be remobilised by particle-associated grazers (see S-Animation, Figure 3), illustrating how abiotic/biotic transformations interact[43]. This combination of abiotic and biotic

processes, along with the refractory nature of lithogenic iron[8] (S-Figure 2B), help explain why iron often has longer remineralisation length-scales than other elements. Since many processes jointly set remineralisation length-scales of different elements, incorporating this level of detail into biogeochemical models to more accurately simulate the stoichiometry of nutrient supply is a major future challenge.

Teasing apart abiotic and biotic transformations

Advances in understanding internal cycling and remineralisation indicate that bioactive metals are characterised by more complex transformations than for major elements. Hence, elucidating the individual and interactive effects of biological and chemical transformations on cycling and remineralisation represents a major challenge. In surface waters, a key goal is to differentiate the roles of phytoplankton and microbes (differing metal quotas, fates), and the function of ligands in setting the taxon-specific bioavailability and/or kinetic constraints on the specific acquisition pathways for recycled versus 'new' metals. These processes set the degree of metal retention and recycling (versus export). Research into iron is most advanced, but we contend that this cannot be used as a biogeochemical template for all trace metals. Other metals, often with different characteristics linked with unique biochemical roles[8,13] and taxon-specific needs[39], require dedicated study and modelling.

At depth, mixed lithogenic/biogenic particle populations, and their varying degrees of metal remobilisation, pose a major challenge to determine whether sinking particles mainly represent a throughput of metals to depth or a vector for the replenishment of dissolved metal inventories (in conjunction with the essential resupply of ligands which retain the

metals in solution[17]). The specific fate of elements within particles also influences the coupling between major and trace elements. Elemental and isotopic mapping of particles, along with biogeochemical models, are powerful approaches to tease apart this puzzle. However, models presently focus on large scales[24], limiting their utility in exploring underlying biogeochemical processes in detail. We advocate a parallel approach, whereby the next generation of biogeochemical models are used within simplified physical oceanographic frameworks to develop new representations of metal cycling and assess the biogeochemical significance of these complex transformations. Models would then reflect both the progress in understanding external sources of metals[5,6], their biogeochemical cycling and the associated return pathways, encapsulated by the term remineralisation, in the oceans' interior.

References

1. Boyd, P.W. et al. A synthesis of mesoscale iron-enrichment experiments 1993-2005: key findings and implications for ocean biogeochemistry. *Science* **315**, 612-617 (2007).

2. Moore, C.M et al. Processes and patterns of oceanic nutrient limitation. *Nature Geosci.* **6**, 701-710 (2013)

3. Cullen, J. T. & Sherrell, R. M. Effects of dissolved carbon dioxide, zinc, and manganese on the cadmium to phosphorus ratio in natural phytoplankton assemblages. *Limnol*. Oceanogr. **50**, 1193–1204 (2005).

4. Koch, F. et al. The effect of vitamin B 12 on phytoplankton growth and community structure in the Gulf of Alaska. *Limnol. Oceanogr.* **56**, 1023-1034 (2011).

5. Jickells, T.D. & C.M. Moore. The importance of atmospheric deposition for oceanic productivity. *Annu. Rev. Ecol. Evol. Syst.* **46**, 481–501 (2015).

6. Resing, J. A. et al. Basin-scale transport of hydrothermal dissolved metals across the South Pacific Ocean. *Nature*, **523**, 200–203. (2015).

7. Fitzsimmons, J.N. et al. Daily to decadal variability of size-fractionated iron and iron-binding ligands at the Hawaii Ocean Time-series Station ALOHA. *Geochim. Cosmochim. Acta* **171**, 303–324 (2015).

8. Twining, B.S., Rauschenberg, S., Morton, P. & Vogt, S. Metal contents of phytoplankton and labile particulate material in the North Atlantic Ocean. *Prog. Oceanogr.* **137**, 261-293 (2015)

9. Karl, D. M. et al. in *Ocean Biogeochemistry: The Role of the Ocean Carbon Cycle in Global Change* (ed Fasham, M. J. R.) Ch. 11, 239-267 (Springer Berlin Heidelberg, 2003).

10. Weber, T., Cram, J.A., Leung S.W., DeVries T. & Deutsch C. Deep ocean nutrients imply large latitudinal variation in particle transfer efficiency. *Proc. Natl. Acad. Sci.* **113**, 8606–8611 (2016).

11. Bruland, K. W. & Lohan, M. C. in *The Oceans and Marine Geochemistry: Treatise on Geochemistry*, (ed Elderfield H.) Ch. 6.02, 23–47. (Elsevier, 2003).

12. Zehr, J. P. & Ward, B. B. Nitrogen Cycling in the Ocean: New Perspectives on Processes and Paradigms. *Appl. Environ. Microbiol.* **68**, 1015-1024. (2002)

13. Morel, F. M. M. & Price, N.M. The biogeochemical cycles of trace metals in the oceans. *Science* **300**, 944–947 (2003).

14. Quigg, A., Irwin, A.J. & Finkel, Z.V. Evolutionary inheritance of elemental stoichiometry in phytoplankton. *Proc. R. Soc. Lond. [Biol.]*, **278**, 526-534 (2011).

15. Singh, A., Baer, S. E., Riebesell, U., Martiny, A. C. & Lomas, M. W. C : N : P stoichiometry at the Bermuda Atlantic Time-series Study station in the North Atlantic Ocean *Biogeosciences*, **12**, 6389-6403 (2015).

16. Martiny, A.C., Kathuria, S. K. & Berube P. Widespread metabolic potential for nitrite and nitrate assimilation among Prochlorococcus ecotypes. *Proc. Natl. Acad. Sci.* **106**, 10787-10792 (2009).

17. Boyd, P.W. & Ellwood, M.J. The biogeochemical cycle of iron in the ocean. *Nature* Geosci. **3**, 675-682 (2010).

18. http://www.geotraces.org/

19. Boyd, P.W. et al. Microbial control of diatom bloom dynamics in the open ocean. *Geophys. Res. Lett.* **39** L18601 (2012).

20. Bowie. A.R et al. Iron budgets for three distinct biogeochemical sites around the Kerguelen Archipelago (Southern Ocean) during the natural fertilisation study, KEOPS-2. *Biogeosciences* **12**, 4421–4445 (2015).

21. Fitzsimmons, J. N., Bundy, R. M., Al-Subiai, S. N., Barbeau, K. A. & Boyle, E. A. The composition of dissolved iron in the dusty surface ocean: An exploration using size-fractionated iron-binding ligands. *Mar. Chem.* **173**, 125-135 (2015).

22. Buck, K. N., Sohst B. & Sedwick, P. N. The organic complexation of dissolved iron along the U.S. GEOTRACES (GA03) North Atlantic Section. *Deep-Sea Res. PT II.* **116**, 152–165 (2015).

23. Aumont, O., Ethé, C., Tagliabue, A., Bopp, L. & Gehlen, M. PISCES-v2: an ocean biogeochemical model for carbon and ecosystem studies *Geosci. Model Dev.* **8**, 2465-2513 (2015).

24 Tagliabue, A. et al. How well do global ocean biogeochemistry models simulate dissolved iron distributions? *Global Biogeochem. Cycles*. **30**, 2015GB005289 (2016).

25. Adly, C. L.et al. Response of heterotrophic bacteria to mesoscale iron enrichment in the northeast subarctic Pacific Ocean. *Limnol. Oceanogr.* **60**, 136–148 (2015).

26. Bundy R. M., Jiang, M., Carter, M & Barbeau, K. A. Iron-Binding Ligands in the Southern California Current System: Mechanistic Studies. *Front. Mar. Sci.* **3**, 27. (2016).

27. Lamborg, C. H., Buesseler, K. O. & Lam, P. J. Sinking fluxes of minor and trace elements in the North Pacific Ocean measured during the VERTIGO program. *Deep-Sea Res. PT II*, **55** 1564–1577 (2008).

28. Sedwick, P. N. et al. Iron in the Sargasso Sea (Bermuda Atlantic Time-series Study region) during summer: Eolian imprint, spatiotemporal variability, and ecological implications. *Global Biogeochem. Cy.* **19**, GB4006 (2005),

29. Boyd, P.W. et al. Why are biotic iron pools uniform across high- and low-iron pelagic ecosystems? *Global Biogeochem. Cy.*, **29**, 1028–1043 (2015)

30. Twining, B.S et al. Differential remineralization of major and trace elements in sinking diatoms. *Limnol. Oceanogr*. **59**, 689–704 (2014).

31. Tagliabue, A., Sallee, J.-B., Bowie, A. R., Levy, M., Swart, S., & Boyd, P. W. Surface-water iron supplies in the Southern Ocean sustained by deep winter mixing. *Nature* Geosci. **7**, 314-320 (2014).

32. Boyd, P.W. & Tagliabue, A. Using the L* concept to explore controls on the relationship between paired ligand and dissolved iron concentrations in the ocean. Mar. Chem. **173**, 52-66 (2015).

33. Bonnain, C., Breitbart, M, & Buck, K. N. The Ferrojan Horse Hypothesis: Iron-Virus Interactions in the Ocean. *Front. Mar. Sci.* **3**, 82 (2016).

34. Wells, M. L., Mayer, L. M., Donard, O. F. X., de Souza Sierra, M. M. & Ackelson, S. G. The photolysis of colloidal iron in the oceans, *Nature* **353**, 248-250 (1991).

35. Barbeau, K. A., & Moffett, J.W. Dissolution of iron oxides by phagotrophic protists: Using a novel method to quantify reaction rates. *Environ. Sci. Technol.* **32**, 2969-2975 (1998).

36. Rubin, M., Berman-Frank, I. & Shaked, Y. Dust-and mineral-iron utilization by the marine dinitrogen-fixer Trichodesmium. *Nature Geosci.* **4**, 529–534 (2011).

37. Hopkinson, B.M. & Barbeau, K. Interactive influences of iron and light limitation on phytoplankton at subsurface chlorophyll maxima in the eastern North Pacific. *Limnol. Oceanogr.* **53**, 1303-1318 (2008).

38. Kirchman D.L. Microbial Ferrous Wheel. *Nature* **383**, 303–304 (1996).

39. Twining, B. S. & Baines S. B. The trace metal composition of marine phytoplankton. *Annu. Rev. Mar. Sci.* **5**, 191–215 (2013).

40. Marchetti, A. et al. Ferritin is used for iron storage in bloom-forming marine pennate diatoms. *Nature*. **457**, 467-470 (2009).

41. Lis, H., Shaked, Y., Kranzler, C. Keren N. & Morel, F. M. M. Iron bioavailability to phytoplankton: an empirical approach. *The ISME Journal*. **9**, 1003-1013 (2015).

42. Sunda W. G. & Huntsman S. A. Iron uptake and growth limitation in oceanic and coastal phytoplankton. *Mar. Chem.* **50**, 189–206 (1995).

43. Melton, C.D., Swanner, E.D., Behrens, S., Schmidt C. & Kappler A. The interplay of microbially mediated and abiotic reactions in the biogeochemical Fe Cycle. *Nat. Rev. Micro.* **12**, 797-808 (2014).

44. Boyd P.W. et al. FeCycle: Attempting an iron biogeochemical budget from a mesoscale SF6 tracer experiment in unperturbed low iron waters. *Global Biogeochem. Cy.* **19** 2005GB002494 (2015).

45. Sarthou, G. et al., The fate of biotic iron during a phytoplankton bloom induced by natural fertilization: Impact of copepod grazing. *Deep Sea Res., PT II*. **55**, 734–751 (2008).

46. Smith, D. C., Simon, M., Alldredge, A.L. & Azam F. Intense hydrolytic enzyme activity on marine aggregates and implications for rapid particle dissolution. *Nature* **359**, 139–142, (1992).

47. Frew, R. D. et al. Particulate iron dynamics during FeCycle in subantarctic waters southeast of New Zealand. *Global Biogeochem. Cy.* **20**, 2005GB002558 (2006)

48. Bidle, K. D. & Azam, F. Accelerated dissolution of diatom silica by marine bacterial assemblages. *Nature* **397**, 508–512, (1999).

49. Clegg, S.L. & Whitfield, M. A generalized model for the scavenging of trace metals in the open ocean—II. Thorium scavenging. Deep Sea Res. **38**, 91–120 (1991).

50. Boyd, P.W. & Trull, T. W. Understanding the export of biogenic particles in oceanic waters: Is there consensus? *Prog. Oceanogr.* **72**, 276–312 (2007).

Corresponding Author

Correspondence and requests for materials should be addressed to Philip Boyd via Philip.boyd@utas.edu.au.

Acknowledgements

The authors thank G. Jackson (Texas A&M University) and T. Kiørboe (Technical University of Denmark) for provision of unpublished data/video footage. The sinking particles presented in Supplemental Figure 2C were collected by Z. Baumann (University of Connecticut) and analysed with the assistance of D. Ohnemus (Bigelow Laboratory for Ocean Sciences). This analysis used resources of the Advanced Photon Source, a U.S. Department of Energy (DOE) Office of Science User Facility operated for the DOE Office of Science by Argonne National Laboratory under Contract No. DE-AC02-06CH11357. Support was provided by Australian Research Council Australian Laureate Fellowship project FL160100131 and Antarctic Climate and Ecosystems Cooperative Research Centre funding to P.W.B., and Australian Research Council Discovery Project DP130100679 to M.J.E. and P.W.B. B.S.T. was supported by US National Science Foundation grant OCE-1232814. Model simulations by A.T. are supported by N8 HPC Centre of Excellence, provided and funded by the N8 consortium and EPSRC (Grant No.EP/K000225/1).

Author contributions

P.W.B., M.J.E., A.T. and B.S.T. contributed equally to conceiving and developing the material presented, and to writing the paper.

Corresponding Author

Correspondence and requests for materials should be addressed to Philip Boyd via Philip.boyd@utas.edu.au.

Competing financial interests

The authors declare no competing financial interests.

Display items

Figure 1 Schematic of modes of 'new' iron supply (orange arrows) and iron retention mechanisms within the surface mixed-layer. Abiotic retention includes rapid transfer of aerosol iron to soluble pools (i.e., Cascade[7]); and photochemically-mediated colloid dissolution[34]. Biotic retention is driven by acquisition (e.g., aerosol capture by diazotrophs[36]) and interactions between iron supply, differing iron quotas (pmol L^{-1}) within natural communities (left-to-right, diatom[39], autotrophic flagellate[39], picoprokaryote[39], picoeukaryote[39], heterotrophic bacterium[39]), and their fate (export (downwards arrow) or grazing/lysis (circle)). Microbial ligand (L) release retains metals in solution (i.e., enterobactin siderophore) and is stimulated by 'new' metal supply[25,26]. The virus represents putative iron recycling through progeny phages[33].

Figure 2 Influence of different supply modes on surface mixed-layer iron (black symbols) and the ratio of new versus recycled iron (red symbols). Iron is mainly delivered to a) Kerguelen[20,45] from sustained deep-water supply (blue arrow denotes estimated duration); b) seasonally-oligotrophic subtropical waters[19] from wintertime offshore lateral supply (blue arrow); c) oligotrophic subtropical waters (Bermuda[28], black; Hawaii[7], green (2012 dataset) and blue (2013) symbols) from episodic dust supply (brown arrows). No *f*e ratio estimates were available; d) low-iron subantarctic waters[44] during spring/summer aerosol deposition

(days 250-100). In panels a)/b) observations were extrapolated (blue lines) based on projected seasonality in dissolved iron inventories[23].

Table 1 Synthesis of remineralisation length-scales of trace metals and major elements in the ocean. Length-scales are expressed as (positive) b values (i.e., higher values denote shorter length-scales) using power-law fitting of the vertical attenuation in particle flux[50]). Values are from observed sinking flux of: all particles (i.e., lithogenic/biogenic, 150-500m depth)[27], and diatoms (50-200m)[30]. b) remineralisation length-scales from biogeochemical simulations (100-1000m) using PISCES[23]. #denotes S as a C proxy. *POC and POP are inter-changeable in model runs. Under "Regeneration processes" R denotes remineralisation, S scavenging/sorption, Re redox state, C complexation, O oxygen concentration, M molecular lability, OC organic coatings. '?' denotes uncertainties.

Figure 3 Mechanisms that set the different remineralisation length-scales evident for trace metals and major elements. a) hypothetical remineralisation mechanisms for a sinking diatom (six-sided polygon) based on SXRF element mapping[30] (S is a C proxy[30,39]). Preferential subsurface regeneration of elements is linked to their association with structural/biochemical cellular components (e.g., membranes) and microbial elemental requirements (circle); b) idealised processes acting on sinking heterogeneous particles (lithogenic/biogenic components with different labilities). Particle transformations drive remineralisation (highlighted terms are metal-specific); and c) depth-dependent changes in particle aggregate surface area (bio-optical profiling float data, courtesy George Jackson) which influences local chemistry and microbial processes (S-Animation).

Methods

Collection of aggregate image (displayed in S Fig 2C)

The aggregate was collected from 15m depth in eastern Long Island Sound using an acid-washed GO-FLO bottle. Particulate aggregates in whole water were settled by gravity into small centrifuge tubes and frozen at -20°C. Samples were subsequently thawed and particles gently collected onto acid-washed 10µm pore-size polycarbonate Isopore membrane filters (Millipore). Un-rinsed filters were frozen at -20°C prior to freeze-drying for 24 h. Aggregates were analyzed with synchrotron X-ray fluorescence (SXRF) microscopy at GEOCARS beamline 13IDE at Advanced Photon Source. Samples were held in a He environment and scanned with 10.5 keV incident X-rays focused to approximately 2µm spot with Kirkpatrick-Baez mirrors. A dwell time of 200 msec at each pixel was used.

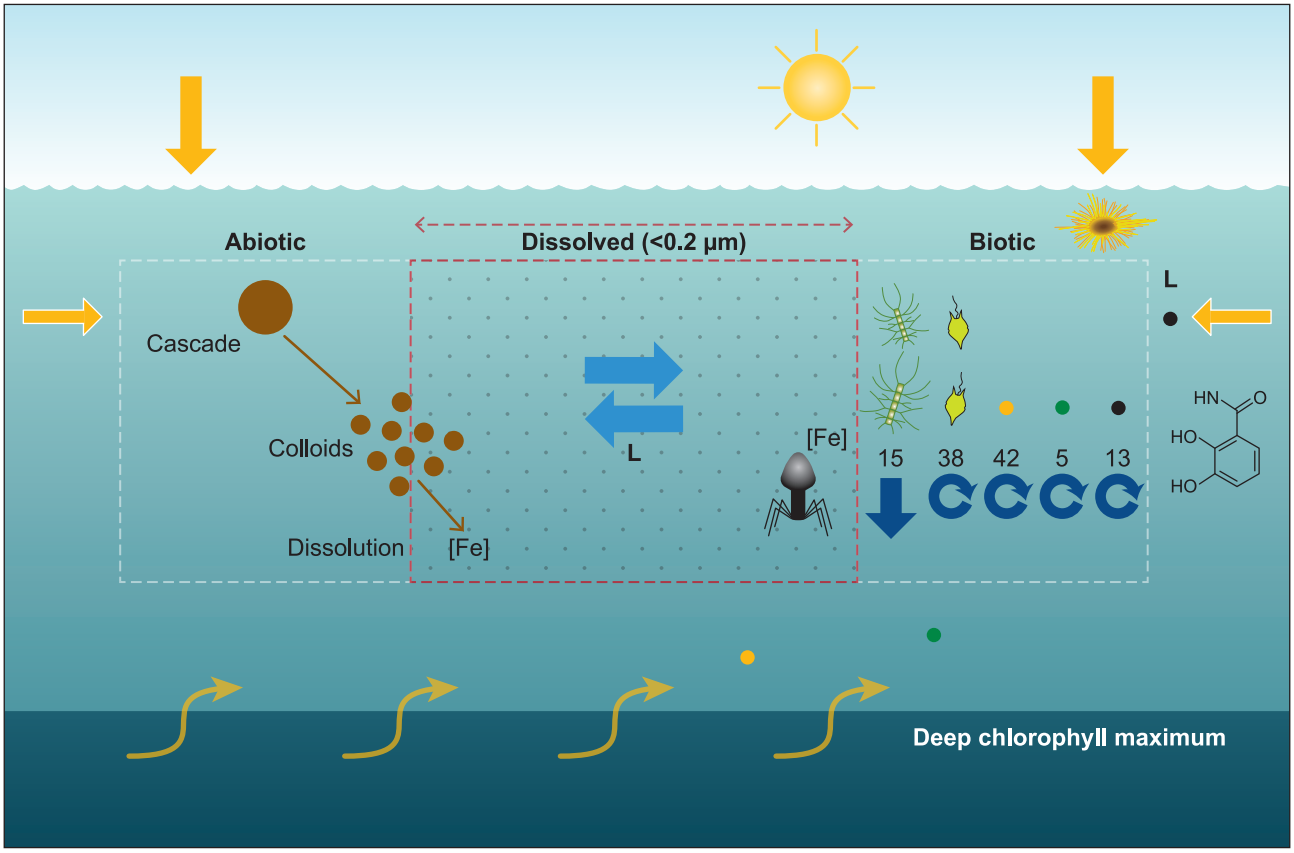
Abiotic
Dissolved (<0.2 µm)
Biotic
L
Cascade
Colloids
Dissolution
[Fe]
L
[Fe]
15
38
42
5
13
HN
O
HO
HO
Deep chlorophyll maximum

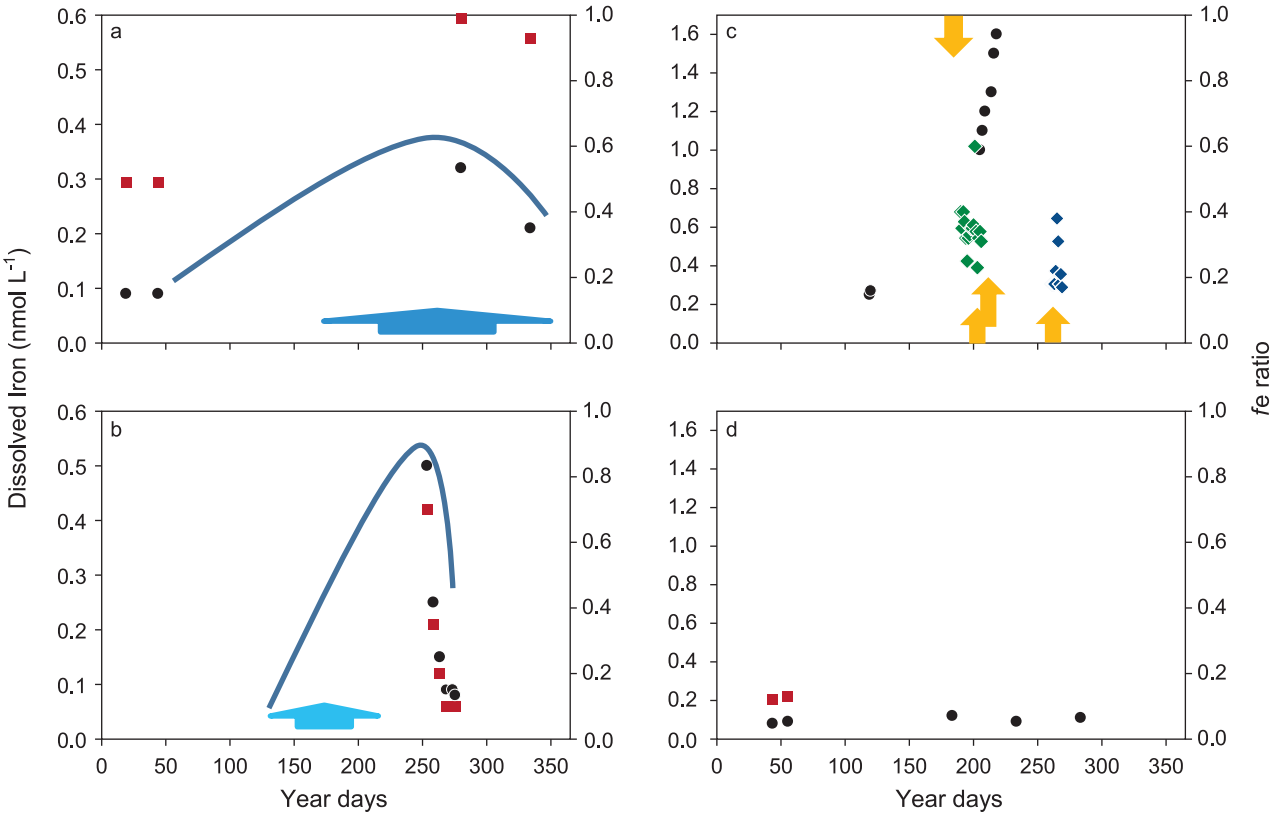
a
b
c
d
Dissolved Iron (nmol L-1)
fe ratio
Year days
Year days
0.0
0.1
0.2
0.3
0.4
0.5
0.6
0.8
1.0
1.2
1.4
1.6
0
50
100
150
200
250
300
350

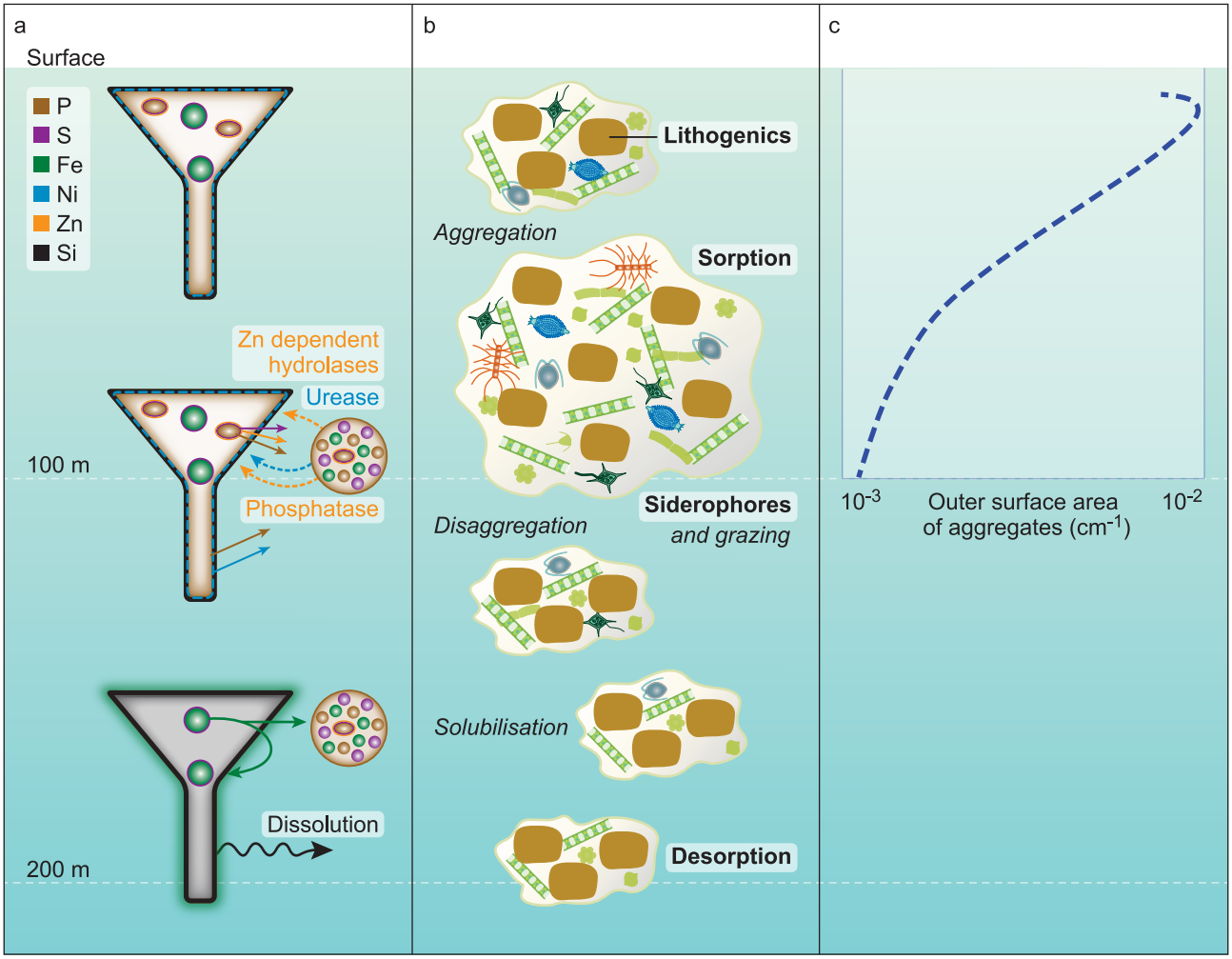
a
Surface
P
S
Fe
Ni
Zn
Si
Zn dependent hydrolases
Urease
Phosphatase
100 m
Dissolution
200 m
b
Lithogenics
Aggregation
Sorption
Siderophores and grazing
Disaggregation
Solubilisation
Desorption
c
10-3
Outer surface area of aggregates (cm-1)
10-2

a)					
Element	**b value**	**Relative difference (scaled to POC)**	**Regeneration processes and factors**	**Particle assemblage**	**Region**
N	1.68±0.13	1.34	R, O, Re	All	North SubTropical Pacific Gyre (NSTPG) (27)
POC	1.25±0.09	1	R, O, M	All	NSTPG
C#	1.09±0.60	1	R, O, M	Diatoms	New Zealand (S Pacific) (30)
P	0.88±0.48	0.70	R	All	NSTPG
P	0.63±0.28	0.58	R	Diatoms	S Pacific
bSi	0.22±0.53	0.18	R, OC	All	NSTPG
Si	0.12±0.11	0.11	R, OC	Diatoms	S Pacific
Zn	0.77±0.34	0.70	R, C?	Diatoms	S Pacific
Ni	0.90±0.76	0.83	R	Diatoms	S Pacific
Al	0.52±0.29	0.42	R, S,	All	NSTPG
Fe	0.32±0.28	0.07	R, S, Re, C	All	NSTPG
Fe	0.13±0.17	0.12	R, S, Re, C	Diatoms	S Pacific
Cu	0.09±0.38	0.07	R, S?, Re?	All	NSTPG
b)					
POC	1.65±0.57	1	R, O	All	Global ocean > 1000 m depth
POP*	1.65±0.57	1	R, O	ditto	ditto
BSi	0.24±0.05	0.15	R,	ditto	ditto
PFe	0.88±0.32	0.53	R, O, S	ditto	ditto

Table 1